TH5A-6

Numerical Evaluation of the Green's Functions for Cylindrical Enclosures by a new Spatial Images Method

P. Vera Castejón, F. Quesada Pereira, D. Cañete Rebenaque, J. Pascual Garcia, A. Alvarez Melcón

***Abstract*— A new and simple spatial images method has been implemented for the numerical calculation of the Green's functions in circular cylindrical enclosures. The technique is based on the imposition of the boundary conditions for the potentials, using a spatial images arrangement. Results show that the numerical convergence of the novel technique is attained fast. They also demonstrate that the new Green's functions lead to accurate results when analyzing real structures. The technique has been used for the efficient analysis of practical planar circuits shielded in circular cavities.**

***Index Terms*— Green functions, Integral Equations, Printed Circuits, Cavities, Circular Waveguide**

I. Introduction

The analysis of shielded circuits and cavity backed antennas is a subject that has attracted recently the attention of many investigations [1]. The main reason for this is the need to create software tools which can evaluate and predict the shielding effects occurring in many Monolithic Microwave Integrated (MMIC) high frequency circuits and cavity backed antennas mounted on vehicles [2].

For the analysis of shielded circuits and cavity backed antennas, the integral equation technique has grown in popularity due to its efficiency, and to the capability to push to a maximum the analytical treatment of the problem [3]. The key element of any integral equation formulation is the ability to compute the Green's functions of the problem.

For the calculation of the Green's functions, only the rectangular enclosure has been extensively treated in the past [4]. For this geometry the Green's functions are usually expressed, using spectral domain formulations, with slow convergence series of vector modal functions inside the rectangular cavity [4]. However, recently attempts have been reported to compute them using spatial domain formulations [5], where the Green's functions are expressed as slow convergence series of spatial images.

Due to this particular mathematical formalism of the Green's functions inside cavities, the circular geometry has been by far less exploited. In general, the Green's functions formulation in circular geometries are based on spectral domain techniques, by using the corresponding vector modal series based on the Bessel functions [6]. However,

Technical University of Cartagena. Campus Muralla del Mar, s/n, E-30202 Cartagena, Spain. E-mail: fernando.quesada@upct.es

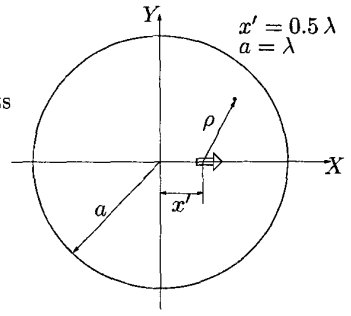

Fig. 1. Unitary dipole inside a circular cylindrical cavity studied in this paper.

this approach shows to be critical from the numerical point of view, since the higher order Bessel functions are not easily computed with high accuracy. Also, since the convergence of the series is slow, very high orders of Bessel functions are usually required. On the other hand, spatial domain formulations have not been applied to the computation of the Green's functions in circular-cylindrical geometries. This is mainly because an analytical solution for the spatial images of a point source in the presence of circular-cylindrical metallic structures does not exist.

In this context, the paper presents a numerical technique that can be used for the computation of the Green's functions in circular-cylindrical cavities. The technique is formulated for the first time in the spatial domain, and it uses the theory of images to enforce the proper boundary conditions for the fields. In this paper the technique is applied to the numerical calculation of the Green's functions inside an empty circular-cylindrical cavity. Its extension, however, to consider dielectric layers inside the cavity is straightforward.

II. Theory

The geometry for the calculation of the mixed potential Green's functions is presented in Fig. 1. As shown, a unit dipole is placed inside a circular-cylindrical metallic cavity. For the electric scalar potential Green's function we should impose null potential on the cavity wall. If we impose this condition at only one point of the wall, then a proper choice will be to place an infinite plane tangent to the cylindrical wall at the point of interest, and then by image theory take a negative charge at the mirror position with respect to the plane.

0-7803-8331-1/04/$20.00 © 2004 IEEE

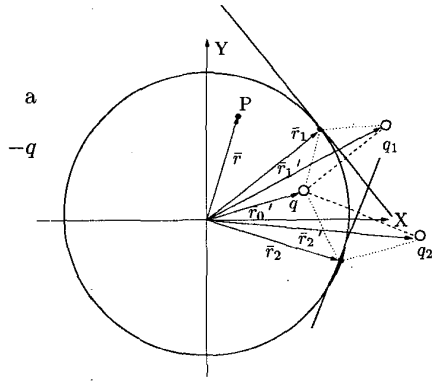

Fig. 2. Image charges rearrangement used to enforce the boundary conditions for the electric scalar potential at discrete points along the cylindrical wall. Point P is a generic observation point.

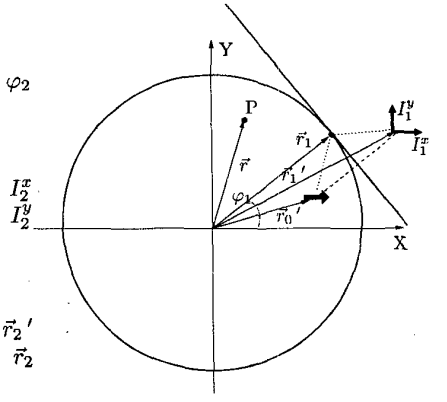

Fig. 3. Image dipoles used to enforce the boundary conditions for the magnetic vector potential at discrete points along the circular cylindrical wall.

It is desirable, however, to be able to impose the boundary conditions at more than one point of the cylindrical wall. To do so we continue with the same strategy, and now we take two tangent planes to the cylindrical cavity in order to impose the boundary conditions at two distinct points (see Fig. 2). The key point of the procedure is to evaluate numerically the value of the two image charges so that the boundary conditions for the potential are satisfied at the two selected tangent points.

The same procedure can now be generalized in order to impose proper boundary conditions for the potential at N distinct points ($\bar{r}_i$) of the cylindrical wall. The following system of linear equations is obtained:

$$\sum_{k=1}^{N} q_k\, G_V(\bar{r}_i, \bar{r}_k\,') = -G_V(\bar{r}_i, \bar{r}_0\,'); \quad i = 1, 2, \cdots, N \quad (1)$$

where all positions vectors are shown in Fig. 2, and $G_V(\bar{r}, \bar{r}\,')$ is the potential Green's function of a unit point charge in free-space.

The solution of this system gives the value of the N image charges (q_k) needed to satisfy the boundary conditions for the potential at N distinct points of the cylindrical wall. The final scalar potential Green's function inside the cylindrical cavity is simply evaluated by reusing the already computed charge amplitudes:

$$G_{V_{\text{cyl}}}(\bar{r}) = G_V(\bar{r}, \bar{r}_0\,') + \sum_{k=1}^{N} q_k\, G_V(\bar{r}, \bar{r}_k\,') \quad (2)$$

For the evaluation of the magnetic vector potential dyadic Green's function, a similar procedure is followed, but taking into account the vector nature of the quantity to be computed. Considering a unit dipole oriented along the x-axis (Fig. 3), we first impose the boundary conditions at one point of the cylindrical wall. In this case, the zero tangent component of the electric field at the cavity wall leads to two different conditions for the magnetic vector potential:

$$\hat{e}_\rho \times \bar{A} = 0; \qquad \nabla \cdot \bar{A} = 0 \quad (3)$$

Expanding the divergence in cylindrical coordinates, the second condition can be translated to the normal component of the magnetic vector potential in the following way:

$$\frac{1}{\rho}\frac{\partial}{\partial \rho}(\rho A_\rho) = \frac{A_\rho}{\rho} + \frac{\partial A_\rho}{\partial \rho} = 0 \quad (4)$$

To impose both conditions at one point of the cylindrical cavity wall, we propose to use two orthogonally oriented dipoles, each one having different weights, as shown in Fig. 3.

The same procedure can now be generalized in order to impose the right boundary conditions at N-arbitrary points along the cavity wall. Following this technique, a $(2N \times 2N)$ system of linear equations is obtained, namely:

$$-\sin(\varphi_i) \sum_{k=1}^{N} G_A^{xx}(\bar{r}_i, \bar{r}_k\,')\; I_k^x + \cos(\varphi_i) \sum_{k=1}^{N} G_A^{yy}(\bar{r}_i, \bar{r}_k\,')\; I_k^y = \sin(\varphi_i)\; G_A^{xx}(\bar{r}_i, \bar{r}_0\,') \quad (5a)$$

$$+\cos(\varphi_i) \sum_{k=1}^{N} C_{i,k}^x\; I_k^x + \sin(\varphi_i) \sum_{k=1}^{N} C_{i,k}^y\; I_k^y = -\cos(\varphi_i)\; C_{i,0}; \quad i = 1, 2 \cdots N \quad (5b)$$

where we have defined the following constants:

$$C_{i,k}^x = \frac{G_A^{xx}(\bar{r}_i, \bar{r}_k\,')}{\rho} + \hat{e}_\rho \cdot \nabla G_A^{xx}(\bar{r}_i, \bar{r}_k\,') \quad (6a)$$

$$C_{i,k}^y = \frac{G_A^{yy}(\bar{r}_i, \bar{r}_k\,')}{\rho} + \hat{e}_\rho \cdot \nabla G_A^{yy}(\bar{r}_i, \bar{r}_k\,') \quad (6b)$$

Both constants can be computed, for a general multilayered medium, in the spectral domain. For the case of free space, however, straightforward calculations lead to the

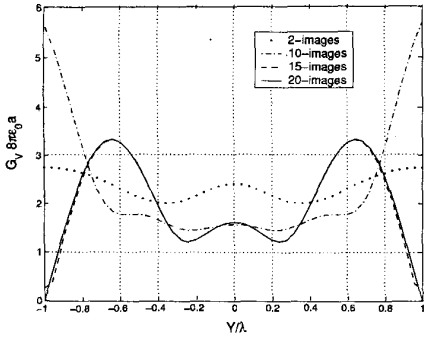

Fig. 4. Electric scalar potential G_V convergence along the Y-axis.

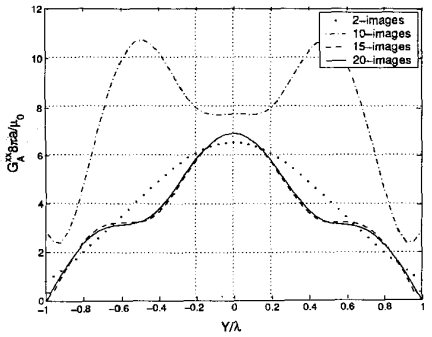

Fig. 5. Magnetic vector potential G_A^{xx} convergence along the Y-axis.

following closed form expression:

$$C_{i,k}^{x} = C_{i,k}^{y} = \frac{\mu_0\, e^{-j\,k_0\,|\bar{r}-\bar{r}_i'|}}{4\pi|\bar{r}-\bar{r}_i'|}\left(\frac{1}{\rho}+\left[\hat{e}_\rho\cdot(\bar{r}-\bar{r}_i')\right]\left[\frac{1}{|\bar{r}-\bar{r}_i'|^2}+\frac{jk_0}{|\bar{r}-\bar{r}_i'|}\right]\right) \tag{7}$$

Once the system is solved, all the amplitudes of the $(2\,N)$ image dipoles (I_k^x, I_k^y) are used to recover the magnetic vector potential components inside the cylindrical cavity, in the following way:

$$G_{A_{\rm cyl}}^{xx}(\bar{r}) = G_A^{xx}(\bar{r},\bar{r_0}') + \sum_{k=1}^{N} I_k^x\; G_A^{xx}(\bar{r},\bar{r_k}') \tag{8a}$$

$$G_{A_{\rm cyl}}^{yx}(\bar{r}) = \sum_{k=1}^{N} I_k^y\; G_A^{yy}(\bar{r},\bar{r_k}') \tag{8b}$$

It is worth mentioning that, according to these expressions, an x-directed dipole will produce a y-component of the magnetic vector potential. This cross component is given by the y-component of the dipole images in the arrangement shown in Fig. 3, and physically it is caused by the curvature nature of the circular-cylindrical cavity wall.

III. Results

In order to check the numerical behavior of the technique developed, we present in Fig. 4 the electric scalar potential Green's function along the Y axis, for a cavity with radius $a = \lambda$ (Fig. 1). The figure shows the results obtained when 2, 10, 15 and 20 points are used to enforce the boundary conditions. It can be observed that the results with 15 and 20 points are very similar, showing that convergence has been reached. It is interesting to note in the figures that the right boundary condition for the electric scalar potential at the cavity wall is satisfied.

Similar results are presented in Fig. 5 for the $G_{A_{\rm cyl}}^{xx}(\bar{r})$ component of the vector magnetic potential dyadic Green's function along the Y-axis. Again the results are presented

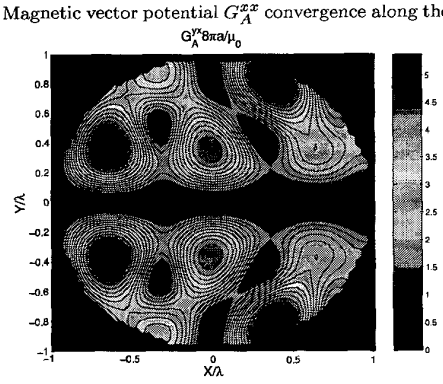

Fig. 6. Magnetic vector potential G_A^{yx} evaluated with 20 images.

when 2, 10, 15, and 20 points are used to enforce the boundary conditions. Also in this case the convergence is attained with about 15 points, showing the effectiveness of the derived approach.

As already discussed, the curvature of the circular-cylindrical cavity generates a cross $G_{A_{\rm cyl}}^{yx}(\bar{r})$ component of the magnetic vector potential dyadic Green's function (see equation (8b)). Fig. 6 presents a contour plot of this $G_{A_{\rm cyl}}^{yx}(\bar{r})$ cross component. It can be observed that this component tends to be maximum at directions 45^o off the horizontal axis, while it is very small along the main X-axis of Fig. 1.

As a validation example, we present in Fig. 7 the $G_{EJ_{\rm cyl}}^{xx}(\bar{r})$ component of the electric field dyadic Green's function, along the Y-axis, as computed with the novel Green's functions formulated in this paper. Furthermore, Fig. 8 shows the cross $G_{EJ_{\rm cyl}}^{yx}(\bar{r})$ component, again along the Y-axis of Fig. 1. In the figures, we include for comparison the results obtained using a standard Surface Integral Equation technique, considering a unitary dipole inside a circular-cylinder of finite height. The surface Integral Equation utilizes the free-space Green's functions, and it discretizes the finite lateral wall of the cylinder using triangular cells. The Integral Equation is solved with a Galerkin procedure, using roof-top basis functions defined on triangular cells. Both figures show the results obtained with the Integral Equation considering two cylinders of different heights $(h/\lambda = 2, 4)$. It can be observed that the field recovered with the newly developed cavity Green's func-

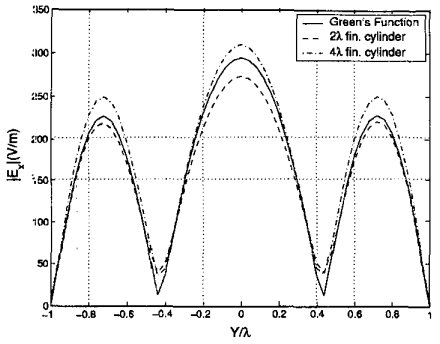

Fig. 7. Electric field $G^{xx}_{E J_{cyl}}(\bar{r})$ component along the Y-axis.

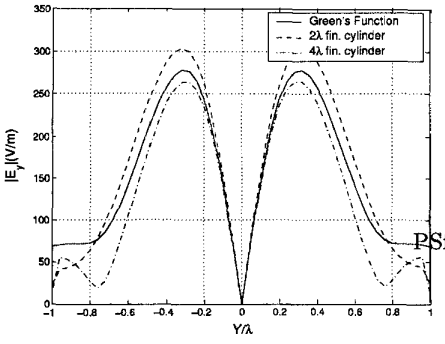

PSfrag replacements

Fig. 8. Electric field $G^{yx}_{E J_{cyl}}(\bar{r})$ component along the Y-axis.

tions is very closed to the field computed with the Integral Equation approach.

For the numerical solution of the Integral Equations in these examples, 844 cells (1211 unknowns) were used in the discretization of the whole lateral cavity wall. On the contrary, the new Green's functions are calculated using 20 points along the wall contour. It is important to point out that, in the novel formulation, the number of points needed to achieve good convergence depends on the electrical size of the cylindrical cavity. Numerical results have shown that good numerical precision is obtained when 15 points are used per wavelength of the cylindrical cavity radius (15 points per a/λ).

As a final example, we have analyzed the square patch shown in Fig. 9, placed inside a circular-cylindrical cavity. Fig. 10 presents the input impedance obtained with the new mixed potential Green's functions formulated in this paper. The integral equation is solved with the Method of Moments, by discretizing the geometry of the patch with triangular cells. In the figure we can compare these results with those obtained using a spectral domain formulation inside a square waveguide of equal area [5]. Also, the results obtained with a free-space integral equation, are included. In this last case, both the patch and the cavity wall (of 20cm height) are discretized using triangular cells. The results using the new Green's functions agree well with those obtained with the other techniques. These results confirm the usefulness of the derived Green's functions for the analysis of real practical structures.

PSfrag replacements

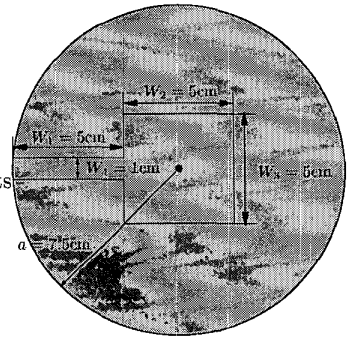

Fig. 9. Patch structure inside a circular enclosure.

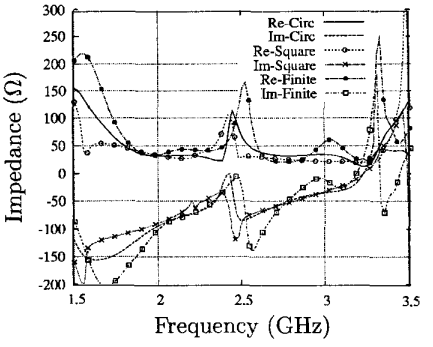

Fig. 10. Input impedance obtained with three different techniques.

IV. Conclusions

In this paper we have presented a simple and efficient procedure to numerically evaluate the Green's functions inside cylindrical cavities. The value of the approach derived is in that it can be used inside integral equation formulations for the analysis and design of shielded circuits and cavity backed antennas inside cylindrical enclosures. The approach is based on the imposition of the boundary conditions for the mixed potential Green's functions at discrete points of the cylindrical cavity wall. This imposition is achieved with the aid of discrete spatial images.

References

[1] L. Dussopt and J.-M. Laheurte, "Cavity-backed antenna integrating a self-oscillating mixer," *Microwave and Optical Technology Letters*, vol. 21, pp. 156–158, April 1999.

[2] R. Faraji-Dana and Y. L. Chow, "Accurate and efficient CAD tool for the design of optimum packaging for (M)MICs," *IEE Proceedings-Microwave Antennas and Propagation*, vol. 142, pp. 81–88, April 1995.

[3] G. G. Gentili, L. E. Garcia-Castillo, M. Salazar-Palma, and F. Perez-Martinez, "Green's funcion analysis of single and stacked rectangular microstrip patch antennas enclosed in a cavity," *IEEE Transactions on Antennas and Propagation*, vol. 45, pp. 573–579, April 1997.

[4] M.-J. Park and S. Nam, "Rapid calculation of the green's function in the shielded planar structures," *IEEE Microwave and Guided Wave Letters*, vol. 7, pp. 326–328, october 1997.

[5] A. A. Melcon, J. R. Mosig, and M. Guglielmi, "Efficient CAD of boxed microwave circuits based on arbitrary rectangular elements," *IEEE Transactions on Microwave Theory and Techniques*, vol. 47, pp. 1045–1058, July 1999.

[6] K. W. Leung and K. Y. Chow, "Analysis of hemispherical cavity-backed slot antenna," *elecl*, vol. 32, pp. 1430–1431, August 1996.